Steady-State Electrochemistry Isolates Electron Hopping from Counterion Diffusion-Migration in Planar MOF Films

Ben A. Johnson[1,*], Ashleigh T. Castner[2], Hemlata Agarwala[1], Sascha Ott[2,*]

[1] *Technical University of Munich (TUM), Campus Straubing for Biotechnology and Sustainability, Uferstraße 53, Straubing 94315, Germany*

[2] *Department of Chemistry – Ångström Laboratory, Uppsala University, Box 523, 75237 Uppsala, Sweden*

*Email: ben.johnson@tum.de, Sascha.Ott@kemi.uu.se

Abstract Current methods for measuring electron-hopping diffusion coefficients of planar metal-organic framework (MOF) films typically use transient potential-step experiments, assuming a simple diffusional response. However, these experiments induce a net flux of counter ions, resulting in an electric field and transport by electromigration, which can impair the accuracy of the measurement. To remedy this, we employ an alternative method based on steady-state cyclic voltammetry. By adding a mobile redox acceptor molecule to the electrolyte, the additional cross reaction between the film and the acceptor mimics a source-drain electrode configuration, generating a steady state with negligible counter ion flux. Additionally, we construct a bespoke physical model and derive an analytical expression to correct the current response for any electric field effects. Overall, this method effectively isolates the diffusional response from ionic diffusion-migration and electric field effects. We expect these results will improve the accuracy of experimentally determined electron-hopping rates of electroactive MOF films.

Introduction

Advances in molecular catalysis for energy conversion have reached a point where molecular transition metal complexes are becoming competitive with material-based electrocatalysts in terms of current density and stability.[1–3] Coupled with a tunable ligand environment and high product selectivity, molecules capable of mediating the catalysis of electrochemical reactions are coming closer to being industrially viable.

Crucial to this development is the immobilization of the molecular species in heterogeneous support structures. In such cases, high catalytic currents and fast conversion of substrate to product require a high density of active sites, and thus any suitable support scaffold must exhibit a high surface area.[4] Metal-organic frameworks (MOFs) are a class of materials with record high internal surface areas[5] and have the capability to host high densities of molecular catalysts into their structures.

Concerning MOF-based catalysis with discrete and molecularly defined redox catalysts, it is well known that both mass and charge transport operate via diffusional processes.[6–9] Electron hopping or self exchange behaves formally as the diffusion of electrons between fixed redox-active linkers.[10,11] Consequently, the practical deployment of such materials hinges upon diffusional charge and mass transport operating faster than the intrinsic catalytic rate for the system to function with high effectiveness.[12] Thus, developing quantitative strategies for accurately benchmarking catalysis and charge and mass transport in these materials is an important endeavor.[4,12]

One major effort in this direction has been quantifying the rate of electron-hopping diffusion for a variety of redox-active MOFs.[13–16] Potential-step experiments are most widely used, where the resulting short-time response is fit to various forms of the Cottrell equation[17] to extract an apparent electron-hopping diffusion coefficient, D_e^{app}, assuming the only mode of charge transport is semi-infinite linear diffusion, i.e., only processes within the MOF are probed, and the MOF film/electrolyte interface is not explored.

However, the *transient* nature of these measurements, implies a non-zero flux of mobile redox-inactive counter ions across the film (Figure 1a), which is especially evident when the redox active linker concentration greatly exceeds that of the supporting electrolyte (we will show that this is often the case). The unaccounted diffusion-migration of counter ions, which is not considered in the Cottrell equation, leads to a deviation in this measurement compared to the intrinsic electron-hopping diffusion coefficient, which we will call D_e. This variation arises because the measured response (current or otherwise) depends on both the diffusion coefficient of the counter ions (D_I) and any migration effects due to a potential drop across the film. Conversely, in experiments designed to operate under *steady-state* diffusion, the net counter ion flux is zero, and the value of D_I will not affect a measurement of D_e (Figure 1b).

In the 1980's, Murray and co-workers pioneered various methods employing electrode configurations that enforce steady-state diffusion in closely related redox polymers.[18] This involves setting the potential at two ends of the film and measuring the resulting current flow, which under steady-state conditions is simply proportional to $\sim D_e/\ell$ (where ℓ is the distance between the two electrodes). Aptly named "sandwich electrodes" were specially developed for this task.[19] Now, however, commercially available inter-digitated array electrodes (IDA) achieve the same result and are

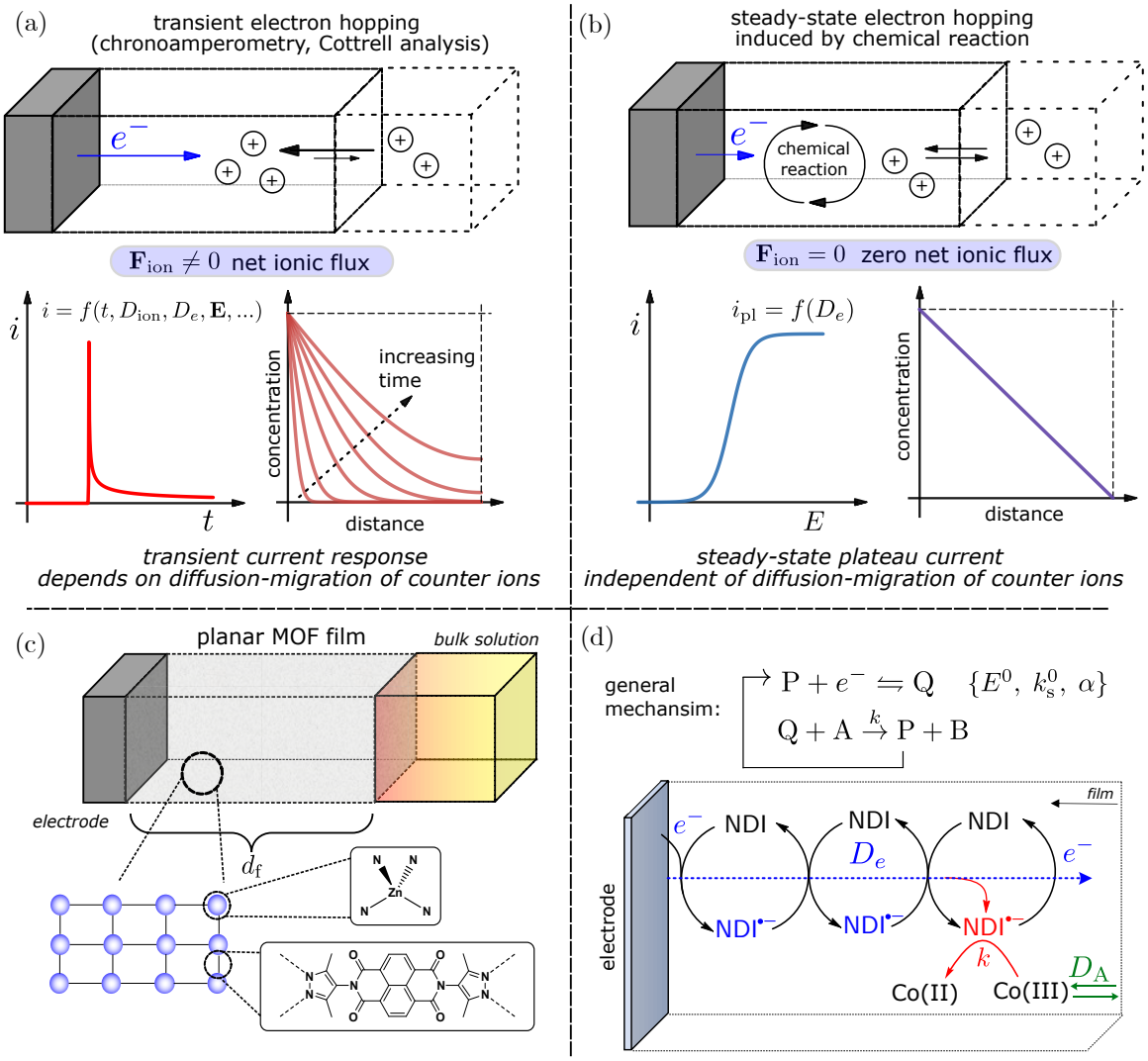

Figure 1: (a) Example of a transient electrochemical method used to measure electron-hopping diffusion coefficients for planar MOF films. This generally consists of monitoring the response of the film after a large potential step (chronoamperometry, chronocoulometry, chronoabsorptometry), followed by application of the Cottrell equation. Such transient methods are characterized by a non-zero net flux ($\mathbf{F}_{\text{ion}}$) for the diffusion-migration of counter ions across the film. The resulting current response is not completely described by the Cottrell equation, and the current is a function of both the counter ion diffusion coefficient D_{I} and the electron-hopping diffusion coefficient D_{e}. (b) A steady-state electrochemical method presented here for extracting D_{e} from planar films, where $\mathbf{F}_{\text{ion}}$ is zero. Steady-state is induced by mutual competition between electron-hopping diffusion and a chemical reaction (in this case single electron transfer with a freely diffusing acceptor). The resulting concentration profiles and current response are time-independent with a plateau current having minimal interference from D_{I}, which can be used to extract D_{e}. (c) Schematic structure of planar Zn(NDI)@FTO MOF films used (with film thickness given by d_{f}), showing the chemical structure of the linkers (dipyrazolate naphthalenediimide) and nodes (tetrahedral Zn). (d) Irreversible catalytic-type reaction mechanism involving outer-sphere electron transfer from the reduced linkers (Q) in Zn(NDI)@FTO to freely diffusing $[\text{Co(bpy)}_3]^{3+}$ (A) with an intra-MOF diffusion coefficient D_{A}. This is termed a "cross-exchange reaction" characterized by a second order rate constant k. Other parameters are listed that describe interfacial electron transfer between the underlying FTO electrode and the oxidized/reduced linkers (P and Q respectively): E^0 is the formal potential of the P/Q couple, k_{s}^0 is the standard heterogenous rate constant, and α is the transfer coefficient.

more commonly used,[20,21] despite sounding much less appetizing.

Interfacing micro-crystalline MOFs with an IDA electrode faces several challenges. Drop-casting, as is done with redox polymers, from a MOF particle suspension typically yields a loosely bound collection of physiosorbed crystallites, with large void spaces. Binder additives are counterproductive because this strategy changes the conductive properties of the resulting composite film. Ideally the MOF should be grown directly onto the IDA electrodes via solvothermal synthesis. MOF growth would need to take place uniformly on both the conductive fingers (typical a noble metal) as well as the non-conductive glass sub-

strate. Differing surface-level interactions[22,23] and rates of nucleation on different substrates, typical of MOF crystallization even under controlled conditions,[24] may disrupt the growth of a homogenous film.

While steady-state measurements of electron-hopping diffusion coefficients are prevalent in the redox-polymer literature, these techniques have yet to be applied to redox-active MOFs, likely for the reason stated above. Consequently, most values for electron hopping diffusion that are obtained by transient measurements of planar films are reported as *apparent* electron diffusion coefficients D_e^{app}, to reflect the fact that electron diffusion is affected by a *net flux of counter ions*, which importantly is also not present during catalytic operation – typically also at steady-state.

Herein, we develop an electrochemical methodology for steady-state measurements of electron-hopping diffusion coefficients compatible with planar redox-active MOF films. By adding a freely diffusing redox-acceptor molecule in the electrolyte, we show that the electron-transfer reaction between the redox-active linkers in the MOF and the mobile acceptor creates the desired steady-state condition, and the current response is proportional to D_e (Figure 1b). This approach was first proposed by Faulkner and co-workers,[25] who were investigating electron transport through copolymer films containing electrostatically bound $[Os(bpy)_3]^{2+}$ (bpy = 2,2′-bipyridyl). They were, however, unable to find an appropriate acceptor/substrate molecule and resorted to a ring-disk dual electrode, similar to an IDA configuration.

Under steady-state conditions induced by the electron transfer reaction, the current response does not depend on the mobile counter ion diffusivity D_I; however, the electromigration component of the electron-hopping process will still need to be accounted for if a considerable electric field builds up within the film. This will be the case whenever the total concentration of the redox-active linkers C_P^0 exceeds that of the mobile counter ions C_I^0. Completely analogous to homogenous molecular electrochemistry, an excess concentration of supporting electrolyte compared to that of the analyte molecule will ensure charges are effectively screened in the diffusion layer, resulting in a negligible electrostatic potential gradient, such that there is no contribution from migration to mass transport of the analyte. For MOF films, due to their high surface area, the effective concentration of linkers is large, typically on the order of the supporting electrolyte concentration (0.1 M – 1 M), and we can expect a significant contribution from electromigration to both electron-hopping and mass transport of mobile counter ions in the film.

Considering these additional processes, our efforts also turned to developing a physico-mathematical model that corrects the current response for any field effects due to migration. This allows us to more accurately extract D_e from data obtained with the steady-state experiments described above. The model presented herein is valid for *planar films*, and it *incorporates migration into both the flux of mobile counter ions and electron hopping* (formally the migration-diffusion of fixed redox-active linkers).

At this stage, differentiating the *intrinsic* diffusion coefficient D_e from an apparent diffusion coefficient D_e^{app} is crucial. The latter is often derived through simple fitting of the Cottrell equation to the transient decay of the current response. This distinction is essential because the assumption that transport is solely governed by semi-infinite electron-hopping diffusion is unlikely to hold for most MOF systems in transient potential step experiments. Herein, we define the parameter D_e to only reflect the underlying microscopic electron hopping process. Conversely, we use D_e^{app} to denote a value obtained by a measurement that includes other effects associated with macroscopic transport. This includes the abovementioned counter ion diffusion and electric field effects leading to interference from electromigrtaion. In other words, D_e^{app} is a function of multiple parameters, $D_e^{app} = f(D_I, D_e, \mathbf{E}, \dots)$, where, for example, $\mathbf{E}$ is the electric field within the MOF film.

For this study, we chose a previously reported Zn-based MOF with naphthalenediimide (NDI) linkers (Figure 1c) and 16 Å wide 1D channels (Zn(NDI)@FTO).[26,27] In our hands, this material forms homogenous thin films on fluorine-doped tin oxide (FTO) substrates (characterized by SEM, and PXRD, Figure S3) and gives a well-defined electrochemical response,[28,29] making it an ideal model platform. In principle, it is possible to monitor the electron transfer reaction from the reduced NDI linkers in the MOF film to a mobile redox couple using standard electroanalytical methods. Here, we chose $[Co(bpy)_3]^{3+}$, which has a formal potential sufficiently positive of that of the NDI linkers to render the mediated reduction of the complex by the film irreversible. The size of $[Co(bpy)_3]^{3+}$ (approximately 11 Å, obtained form the crystal structure)[30] is smaller than that of the pores of the MOF (16 Å).[27]

The overall reaction sequence is displayed in Figure 1d and matches that of a simple one-step, one-electron catalytic mechanism, with P and Q being the oxidized and reduced form of the NDI linker, respectively. The following analysis was performed by varying both the scan rate and the bulk $[Co(bpy)_3]^{3+}$ concentration for films obtained with thicknesses, $d_f = 1$ μm, as measured by SEM images of film cross sections (Figure S3b).

We begin by reiterating the influence of electron-hopping diffusion in MOF films on heterogenized molecular catalysis with a quantitative theoretical examination. Next we evaluate the electron-hopping characteristics of Zn(NDI)@FTO by the common transient methods outlined above. This is followed by a systematic electroanalytical investigation of Zn(NDI)@FTO in the presence of $[Co(bpy)_3]^{3+}$. We then derive an analytical expression using a physico-mathematical model to correct for any field effects on the current response, which allows us to extract a value for D_e under steady-state conditions. We end

with a discussion of the merits of the steady-state technique presented here compared to the more commonly used transient methods, the consideration of diffusion-migration in these experiments, and its implications for molecular catalysis in MOFs.

1 Results and Discussion

Revisiting the importance of D_e in the context of molecular catalysis. For MOF-based molecular catalysis, a common question arises: *is electron-hopping adequately fast to drive catalysis?*[6,31] Naturally, this will depend on D_e, but also the film thickness and catalytic rate.[12] A quantitative answer can easily be obtained by simple scaling arguments for reaction-diffusion. Diffusion coefficients factor into the Damköhler number (Da_e),[32] also referred to as the Thiele modulus,[33] defined here for charge transport as

$$Da_e = d_f^2 \frac{kC_A^0}{D_e}, \tag{1}$$

which is a dimensionless measurement of the competition between the catalytic reaction and electron-hopping diffusion[34,35] (where d_f is the film thickness, C_A^0 is the bulk substrate concentration, and k is the second order rate constant of the catalytic reaction). More specifically, Eq. 1 is the ratio between the timescale for the catalytic reaction, characterized by the reciprocal of the pseudo first-order rate constant, $t_{rxn} = 1/kC_A^0$, and the diffusion time for electrons in the film, $t_d = d_f^2/D_e$.

When $Da_e \ll 1$ or $t_d \ll t_{rxn}$, electrons are supplied to the active sites in the film by diffusion at a sufficient rate, such that the catalytic reaction takes place throughout the entire volume of the film, and the resulting current is simply

$$i = FkC_A^0 C_P^0 V_{film}, \tag{2}$$

where F is Faraday's constant, C_P^0 is the molecular catalyst concentration in the MOF, and V_{film} is the volume of the film, often approximated by the product of its surface area S and thickness d_f, $V_{film} = Sd_f$. This situation in the film is completely analogous to uniform homogenous conditions, for example in a continuously stirred tank reactor.[36]

However, when $Da_e \gg 1$ or $t_d \gg t_{rxn}$, the catalytic reaction occurs faster than the diffusion timescale for electron-hopping. *This does not necessarily mean that diffusion is "rate-limiting,"* as is often invoked. The resultant situation is one where on the fast catalytic timescale, diffusion is only capable of supplying electrons a finite distance within the film, which is much less than the thickness of the film itself. Consequently, the concentration of the active catalyst is depleted, and the reaction no longer occurs homogenously throughout the film. In fact, the reaction is confined to a thin boundary layer of thickness δ_r, proportional to the square-root of the electron-hopping diffusion coefficient:

$$\delta_r = \sqrt{\frac{D_e}{kC_A^0}}. \tag{3}$$

Now, it is appropriate to think of the reaction taking place approximately within a volume given by $V_\delta = S\delta_r$, such that

$$V_\delta = S\sqrt{\frac{D_e}{kC_A^0}}. \tag{4}$$

Replacing the film volume in Eq. 2 with V_δ gives the current response for when electron-hopping is slow compared to catalysis:

$$i = FSC_P^0\sqrt{kC_A^0 D_e}. \tag{5}$$

It follows that *the current is dependent on both the electron hopping diffusion coefficient and the catalytic rate constant* and independent of the film thickness. This situation is analogous to homogeneous molecular catalysis of electrochemical reactions.[37,38]

The important conclusion to draw is that if diffusion is slow, the film losses catalytic effectiveness because the reaction volume is smaller compared to when diffusion is fast, i.e., $V_\delta < V_{film}$. Thus, for a given film thickness and reaction rate, a sufficiently large D_e is often desirable such that the effective reaction volume within the film is as large as possible, and there are few inactive catalytic sites. For maximum catalytic effectiveness $V_\delta \geq V_{film}$, which implies

$$D_e \geq d_f^2 kC_A^0. \tag{6}$$

This condition can also be directly inferred from the Damkhöler number (Eq. 1). How large D_e must be of course also depends on the application. If a higher overall conversion rate of substrate to product is the target, thicker films will be required. Consequently, to avoid loss in catalytic effectiveness, the constraint on the lower limit of D_e adjusts according to the inequality in Eq. 6.

Electrochemical characterization of Zn(NDI)@FTO films by transient methods. The electrochemical response of the Zn(NDI)@FTO films was first investigated in the absence of $[Co(bpy)_3]^{3+}$. We employed the popular Cottrell analysis utilizing a large potential step recorded in DMF with 0.5 M $LiClO_4$ as the supporting electrolyte. At short time points following this potential step, the time-dependent current response is approximately linearly proportional to $t^{-1/2}$. The slope of this linear region was used to calculate D_e^{app} (See Supporting Information, Figures S4 and S5). It was determined from transient chronoamperometry that $D_e^{app} = 2.5 \times 10^{-9}$ cm^2 s^{-1}. Again, the notation here, D_e^{app}, denotes an apparent diffusion coefficient obtained by a transient electrochemical technique combined with simple fitting by the Cottrell equation. These are apparent due to the unaccounted influence of counter ion

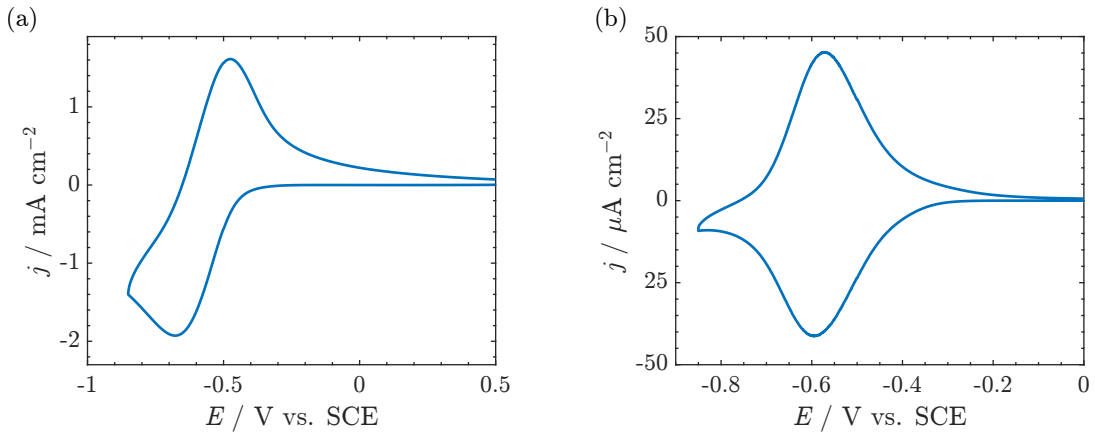

Figure 2: Cyclic voltammograms of Zn(NDI)@FTO in 0.5 M $LiClO_4$/DMF at (a) 200 mV s^{-1} and (b) 1 mV s^{-1}.

diffusion-migration as well as any electric field effects on electron hopping.

We also recorded cyclic voltammograms (CVs) in the absence of $[Co(bpy)_3]^{3+}$, utilizing scan rates spanning more than two orders of magnitude (ν = 1 to 500 mV s^{-1}) (Figure S6a). This gave rise to two visibly different current-potential curves depending on the timescale (Figure 2a-b). At fast scan rates (> 50 mV s^{-1}), a diffusion wave is observed (Figure 2a) with relatively large peak potential separations (ΔE_p = 200 mV at 200 mV s^{-1}) and peak current proportional to $\sqrt{\nu}$ (Figure S6b).

Conversely at slower scan rates (Figure 2b), the wave is symmetric, resembling an adsorption wave, with peak potential separations noticeably less than that for a typical freely diffusing, Nernstian response ($\Delta E_p < 57$ mV).[39]

The fact that both waveforms are accessible with the same electrode material at disparate timescales is indicative of a diffusion process occurring in a *finite domain*, as expected for a multilayer film with discrete redox-active centers, where charge propagates by an outer-sphere electron-hopping mechanism.

Changing the timescale of the voltammogram via the scan rate probes the two limits of diffusion occurring within the film: finite and semi-infinite. The portion of the film that is probed during the CV scan is given by the diffusion layer size

$$\delta_d = \sqrt{\frac{D_e RT}{F\nu}}, \tag{7}$$

where R is the gas constant, F is Faraday constant, T is temperature, and ν is the scan rate. Therefore, the current response is identical to the classical waveform of a monolayer of surface adsorbed species when the diffusion layer size approaches that of the thickness of the film d_f, or when the ratio,

$$l_e = \frac{d_f}{\delta_d} = d_f\sqrt{\frac{F\nu}{D_e RT}}, \tag{8}$$

is less than unity.[39–41] However, electrons are still transported in a formal diffusion process, with the entire film acting as if it were a monolayer on these timescales, with the total surface concentration Γ_P^0 (mol cm^{-2}) given by $\Gamma_P^0 = C_P^0 d_f$, where C_P^0 is the molar concentration (mol cm^{-3}) of NDI linkers in the film. Integration of the current from the cathodic wave at slow scan rates (1 mV s^{-1}, $l_e \ll 1$, Figure 2b) allows us to calculate the redox active surface concentration of NDI linkers as $\Gamma_P^0 = 1.0 \times 10^{-7}$ mol cm^{-2}, which results in a total volumetric concentration of $C_P^0 = 1.0 \times 10^{-3}$ mol cm^{-3} or approximately 1 M.

Current response of Zn(NDI)@FTO in the presence of acceptor. Addition of $[Co(bpy)_3]^{3+}$ to the bulk solution results in the appearance of two new waves: one at approximately −0.12 V and another centered on the formal potential of the NDI linkers at −0.56 V vs. SCE in CVs recorded at 20 mV s^{-1} with Zn(NDI)@FTO (Figure 3a). Increasing the bulk concentration of $[Co(bpy)_3]^{3+}$ (Figure 3b) causes an increase in the current at −0.56 V, and the observed wave changes from reversible and peak-shaped to irreversible with a quasi-plateau.

The current continues to increase until C_A^0 = 24 mM; however, at higher concentrations the plateau current is independent of C_A^0. This contrasts with the wave near −0.12 V, which is peak shaped for all values of C_A^0, and the peak current continuously increases with increasing C_A^0 (Figure S9a). This behavior as well as background scans on bare FTO in the presence of $[Co(bpy)_3]^{3+}$ (Figure S7) allowed us to assign the first wave at −0.12 V as arising from the direct reduction of $[Co(bpy)_3]^{3+}$ at the underlying FTO surface. The second wave (−0.56 V) can be assigned to the mediated reduction of $[Co(bpy)_3]^{3+}$ by the film, given that it exhibits a quasi-sigmoidal response, and the half wave potential ($E_{1/2}$)[42] is centered on E^0 of the NDI linkers (typical of a one-electron process, $E^0 = E_{1/2}$).[37] Importantly, the Co(III)/Co(II) couple (measured on a glassy carbon electrode; Figure S8) appears 800 mV positive of the NDI/NDI$^{\bullet-}$ reduction, resulting in a large driving force for electron transfer, and therefore the cross-reaction between the film and mobile $[Co(bpy)_3]^{3+}$ species can be considered irreversible.

Focusing on only the first wave (−0.12 V) for the

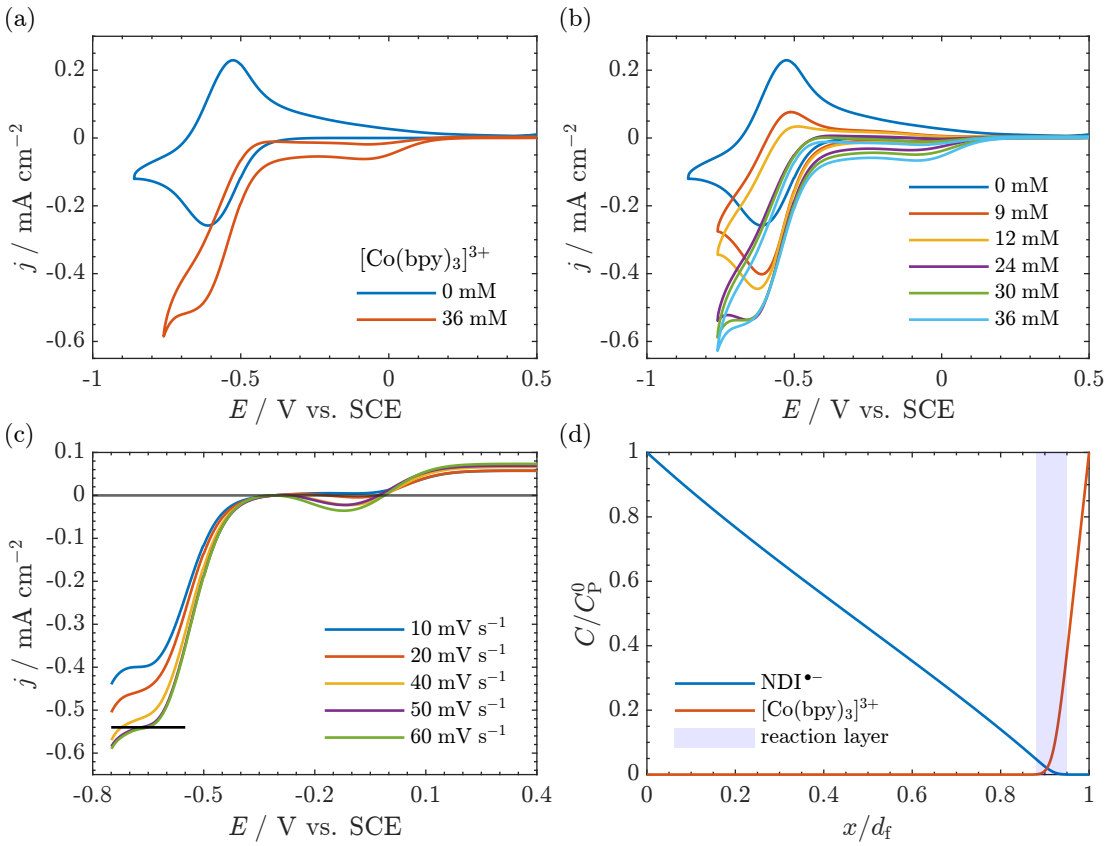

Figure 3: Cyclic voltammograms at 20 mV s^{-1} with 0.5 M $LiClO_4$ in DMF of Zn(NDI)@FTO (a) with [Co(bpy)$_3$]$^{3+}$ (C_A^0= 36 mM) (red) and without (blue) [Co(bpy)$_3$]$^{3+}$, and (b) CVs with increasing concentration of [Co(bpy)$_3$]$^{3+}$ (C_A^0 = 0 mM, blue; 9 mM, red; 12 mM, orange; 24 mM, purple; 30 mM, green; 36 mM, cyan). (c) CVs of Zn(NDI)@FTO with C_A^0 = 36 mM at ν = 10 mV s^{-1} (blue), 20 mV s^{-1} (red), 40 mV s^{-1} (orange), 50 mV s^{-1} (purple), and 60 mV s^{-1} (green). The reverse scan was removed for clarity, and the baseline was corrected to account for the residual current from the first wave by translating the CVs such that the current at the foot of the catalytic wave begins at zero (black line shows the quasi-plateau current at ν = 50 mV s^{-1}). (d) Example dimensionless concentration profiles at the plateau (approximately −0.6 V) showing reduced catalyst Q (blue line, NDI linkers) and acceptor (red line, [Co(bpy)$_3$]$^{3+}$) as a function of distance normalized to the film thickness (x = 0 corresponds to the underlying FTO electrode surface, and $x = d_f$ corresponds to the outer edge of the film at the film-solution interface). Concentration of catalyst and acceptor on the vertical axis is normalized to the total concentration of linkers C_P^0 and bulk acceptor concentration C_A^0 respectively. The thin reaction-layer that develops is highlighted in blue. Concentration profiles were generated from analytical solutions to the physical model presented in the Supporting Information (pp. S18-S19), accounting for diffusion-migration.

moment, in this potential range the MOF is in its neutral state, so the [Co(bpy)$_3$]$^{3+}$ species is essentially diffusing through an inert film to the underlying electrode surface where electron transfer takes place. When the scan rate is decreased, however, a quasi-plateau emerges (Figure S9b). A steady-state voltammetric response is possible for a redox-active species diffusing through an electroinactive layer.[43] This occurs when the diffusion layer thickness of the mobile redox species reaches the size of the inert film and if the diffusion coefficient within the film is significantly less than in the bulk solution. Under these conditions the plateau current is given by

$$i_{pl} = \frac{FSC_A^0 D_A}{d_f}, \qquad (9)$$

where S is the geometric surface area of the film, C_A^0 is the bulk concentration of [Co(bpy)$_3$]$^{3+}$, and D_A is the diffusion coefficient of the acceptor ([Co(bpy)$_3$]$^{3+}$) within the film. Using this analysis, D_A was estimated to be 1.7×10^{-9} cm^2 s^{-1}, which is indeed much smaller than typical diffusion coefficients for small molecules in solution (10^{-5} cm^2 s^{-1}).

We turn now to the nominally catalytic wave corresponding to the mediated reduction of [Co(bpy)$_3$]$^{3+}$ by the MOF film. It should be noted that this reaction is not truly catalytic since the direct reduction of [Co(bpy)$_3$]$^{3+}$ occurs at a more positive potential than its mediated reduction by the film. However, the mechanism given in Figure 1d is certainly that of a catalytic reaction where the cross reaction between the film and [Co(bpy)$_3$]$^{3+}$ is followed by regeneration of the reduced linkers via electron-hopping diffusion.

At high bulk [Co(bpy)$_3$]$^{3+}$ concentrations ($C_A^0 \geq$

36 mM) the plateau current from the sigmoidal current-potential response (at scan rates $\geq 50\ \mathrm{mV\ s^{-1}}$) are approximately scan rate independent (Figure 3c), indicating that the system is under pure kinetic conditions and there is negligible substrate depletion at the film-solution interface.[35,40,44] As mentioned above, the plateau current is also nearly independent of C_{A}^{0} at concentrations greater than 24 mM (Figure 3b).

In the framework of a one-electron catalytic mechanism mediated by a redox film, these two observations uniquely correspond a situation in which, on the timescale of the reaction, the substrate only diffuses a very short distance within the film, and the reaction take place in a thin boundary layer near the film-solution interface.[34,35] This boundary layer is so thin; it can be approximated as a surface reaction. Since no reaction is taking place within the bulk of the film, the concentration profile of reduced catalyst is nearly linear, and the reaction is fast enough ($d_{\mathrm{f}}^{2}kC_{\mathrm{A}}^{0} \gg 1$) to cause the concentration of reduced catalyst to drop to nearly zero at this boundary: $C_{\mathrm{Q}}(x = d_{\mathrm{f}}) \approx 0$ (example concentration profiles are shown in Figure 3d).

This situation arises from a very fast catalytic reaction on the diffusional timescale of both electrons and acceptor. Additionally, the electrons must diffuse further in the film than the acceptor molecule, which requires $D_{\mathrm{A}}C_{\mathrm{A}}^{0} \ll D_{\mathrm{e}}C_{\mathrm{P}}^{0}$.[35] With the high concentration of linker in MOFs, these conditions are relatively easy to meet. The overall result effectively reproduces the steady-state concentration profiles generated with an IDA or sandwich electrode. Here, rather than changing the geometry of the electrode set-up, we are enforcing the desired concentration gradient using a chemical reaction. The underlying electrode surface serves as a "source" of electrons for the film, while the electron transfer reaction with the added acceptor molecule creates a "drain" for electrons at the film-solution interface. A derivation demonstrating how this condition generates the desired concentration profiles is presented in the Supporting Information, pp. S9-S12. It is additionally possible here that the direct reduction of $[\mathrm{Co(bpy)_3}]^{3+}$ at the underlying FTO electrode at potentials more positive of the NDI formal potential (-0.56 V) depletes the acceptor concentration within the film before the catalytic wave is reached. In either case, the plateau current in this situation only depends on the electron transport properties of the film.

Physico-mathematical model and steady-state measurement of D_{e}. The plateau current from Figure 3c is proportional of D_{e}, and in principle will furnish the desired stead-state measurement. However, field effects are likely present due to a non-zero electrostatic potential gradient within the film. To account for the resulting electromigration contribution to electron-hopping, we turned to constructing a physical model to quantitatively describe this process and give us a more accurate determination of D_{e}.

Our model takes into consideration that while electron-hopping in the absence of an electric field is equivalent to simply diffusion, in the presence of an electrostatic potential gradient, the migration contribution to electron-hopping is not the same as that of an ion. That is, the normal Nernst-Planck expression for the flux[45] does not apply. While ion movement is formally monomolecular, electron-hopping is a bimolecular process between discrete redox-active molecules.

This was first enunciated by Savéant,[46] who derived an appropriate extension to the traditional Nernst-Planck equation, which accommodates the bimolecular nature of electron-hopping. This introduces a second order term in the migration component of the flux. While it has been shown to be significant for analyzing redox materials demonstrating electron-hopping,[47] this consideration is sometimes omitted in other models.[48] These models, including ones that have recently gained popularity for investigating charge transport through MOF films,[13,49,50] may have been derived based on assumptions pertinent to materials other than planar films of redox conductors with discrete sites.[29,51] We provide a general summary of Poisson-Nernst-Planck theory as it applies to electron-hopping through redox films in the Supporting Information (pp. S5-S7). Derivations of analytical expressions for the current-potential response, potential gradient within the film as a function of distance, and ionic concentration profiles are also presented in the Supporting Information (pp. S12-S20).

The effect of migration on the current response was first analyzed with voltammograms and concentration profiles generated by the theoretical model (Figure 4). By varying the amount of mobile ionic species (C_{I}^{0}), we found that a low concentration of mobile ions compared with that of the redox-active linkers gives rise to a potential gradient at steady-state within the film (Figure 4b), which induces a corresponding electric field. The direction of the field with respect to the axis perpendicular to the electrode surface is one that repels anions from and attracts cations to the electrode-film interface. In fact, mobile cations are present near the electrode-film interface at higher concentrations than in the bulk electrolyte (Figure 4c).

Furthermore, the dissipative movement of negative charges from electromigration is in the same direction as the diffusional flux arising from the concentration gradient of reduced linkers (Figure 4g; negatively charge species "move up" an electrostatic potential gradient from low to high potential, whereas species tend to "move down" concentration gradients from high to low concentration). The net effect is an enhancement to the overall flux of the electron-hopping process. A higher current response is then observed (Figure 4a, solid line) compared to the case when there is a small or zero potential drop across the film and transport of both electrons and mobile ions are both purely diffusional (Figure 4a, dashed line). As predicted by the analytical model, the current response increases discernibly as mobile ion concentration decrease below that of the redox active linkers (Figure S11).

Consequently, the presence of an electric field and

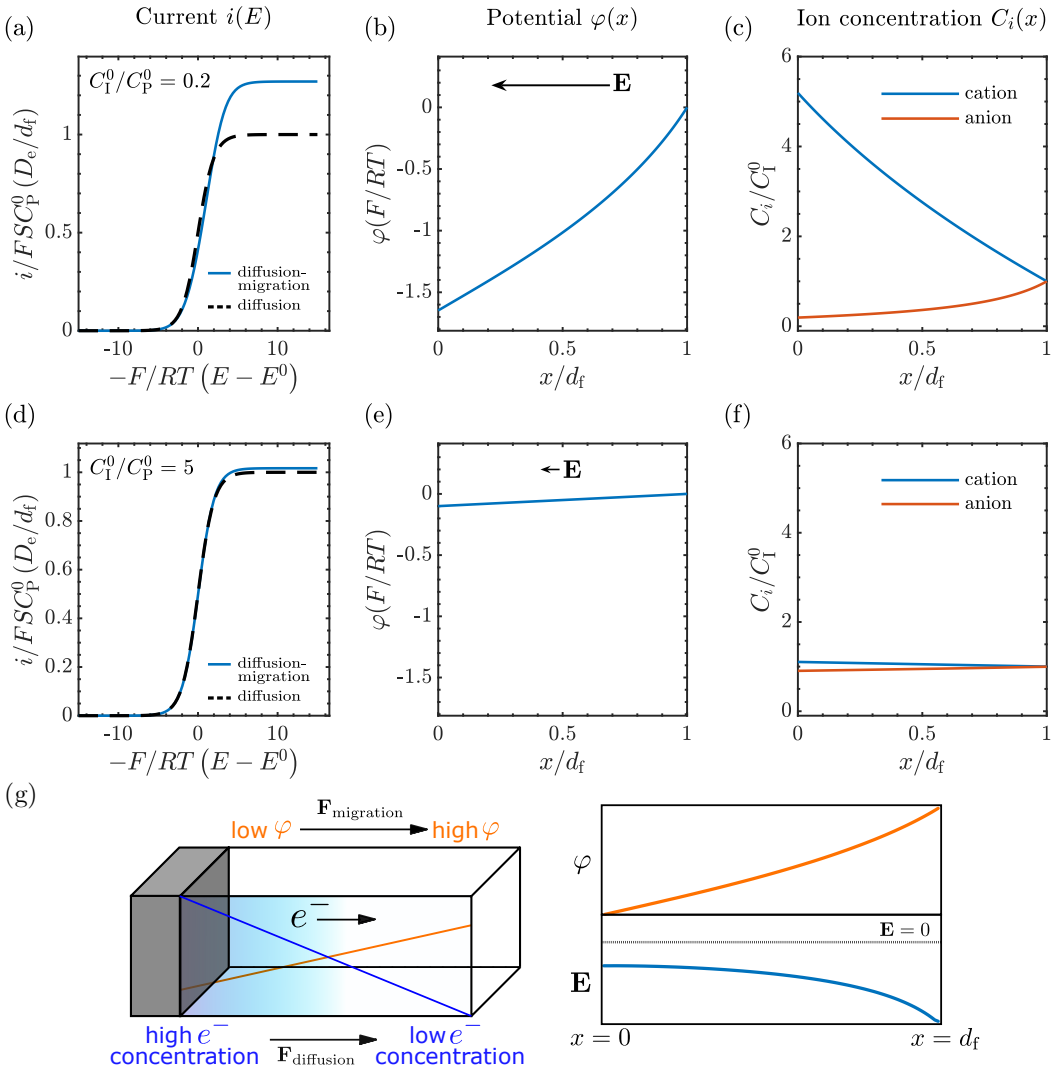

Figure 4: Steady-state catalytic CVs (a,d), electrostatic potential gradient within the film (b,e) and concentration profiles of monovalent mobile cation and anion (c,f) generated by the analytical solution (see Supporting Information, Section 3.4.3). Two different bulk concentrations for the mobile redox-inactive counter ions (considering a neutral binary electrolyte where the bulk anion and cation concentrations are equivalent, given by C_I^0) were used: (a-c) $C_I^0/C_P^0 = 0.2$ corresponding to a weakly supported system ($C_I^0/C_P^0 \ll 1$) and (d-f) $C_I^0/C_P^0 = 5$ corresponding to a fully supported system ($C_I^0/C_P^0 \gg 1$). CVs excluding the effect of migration are shown for comparison (a,d: black dotted line). Accompanying the potential profiles (b,e), the magnitude and direction of the resultant electric field in the film is indicated by a solid arrow. (g) These results are summarized schematically, showing the direction of the total flux for electron-hopping in the film as well as the parallel components arising from migration $\mathbf{F}_{migration}$ (due to the potential gradient, orange line) and from diffusion $\mathbf{F}_{diffusion}$ (due to the concentration gradient of reduced linkers, blue line). The electrostatic potential profile and variation of the electric field (E) as a function of distance in the film are also shown. Other parameters used as input (see Supporting Information, Table S2 for definitions of dimensionless groups): $\Lambda = d_f k_s^0/D_e = 1 \times 10^3$, $\alpha = 0.5$, $z = 0$, where z is the charge on the oxidized linkers, α is the transfer coefficient, k_s^0 is the standard heterogenous rate constant, and Λ is the dimensionless competition parameter for interfacial electron transfer (a surface Damköhler number).

ensuing electromigration resulting from a weakly supported environment in the film (i.e., when $C_I^0/C_P^0 \ll 1$; Figures 4a-c and Figure S11) will cause measurements of D_e to tend to be *overestimated*. If the concentration of mobile ions is higher than the total concentration of redox-active linkers, then the system is fully supported ($C_I^0/C_P^0 \gg 1$) and there is minimal contribution to the current from electromigration (Figures 4d-f and Figure S11). However, this may be difficult to achieve in practice due to the high concentration of linkers (often around 1 M), characteristic of most MOFs.

We then compared the experimental CVs with the current response predicted by the analytical solution (Figure 5). After baseline subtraction to remove the non-catalytic wave (−0.12 V vs. SCE) from the foot of the catalytic current (see Figure S10), this resulted in a steady-state measurement for the electron-hopping diffusion coefficient: $D_e = 5.5 \times 10^{-10}$ cm^2 s^{-1}. Best

fits resulted from using a formal potential for the NDI linkers of $E^0 = -0.5$ V vs. SCE. This is approximately 70 mV positive of the value obtained by experimental CV in the absence of $[Co(bpy)_3]^{3+}$ (Figure 2). We attribute this difference to possible non-ideal intermolecular interactions between the NDI linkers and freely diffusing $Co(bpy)_3$ within the MOF pores. Notably, as shown in the Supporting Information (p. S14), this value for the electron hopping diffusion coefficient D_e minimizes the contribution from ionic diffusion (independent of D_I) and is corrected for any field effects arising from electromigration.

Two key assumptions used in the analytical model and the method overall are: 1) the thin reaction layer is positioned next to the film-solution interface, meaning electrons must diffuse further than the acceptor; and 2) the electron transfer reaction between the linkers and acceptor molecule is fast relative to the diffusion timescales for both electrons and acceptor. These conditions generate concentration profiles that mimic those obtained by an IDA electrode (Figure 3d). The first assumption is valid when $D_A C_A^0 / D_e C_P^0 \ll 1$. Given the experimentally determined magnitudes of D_e (10^{-10} cm^2 s^{-1}) and D_A (10^{-9} cm^2 s^{-1}), as well as the relative ratio of linker concentration to acceptor concentration, we indeed find $D_A C_A^0 / D_e C_P^0 = 0.1 \ll 1$. The physical meaning of this result is discussed in more detail in Section 3.3.3 of the Supporting Information (p. S8).

Regarding the fast rate of electron transfer between linker and acceptor, we could corroborate this by utilizing the experimentally determined values of the diffusion coefficients to estimate a lower bound on the cross-exchange rate constant k for electron transfer between the $NDI^{\bullet-}$ linkers and $[Co(bpy)_3]^{3+}$ (see Supporting Information, Section 4.1, p. S16 for details of this calculation). The conditions that produce the desired concentration profiles (Figure 3d) would require $k \geq 10^2$ M^{-1} s^{-1}. With a large driving force of approximately 0.8 V, this reaction is likely to proceed at this rate or faster. Applying Marcus theory for outer sphere electron transfer to calculate an approximate value for k confirms this. Reorganization energies were obtained by density functional theory (DFT), which, in conjunction with the Marcus cross relation, yields $k \approx 6 \times 10^7$ M^{-1} s^{-1} (for more details, see Supporting Information, Section 4.2, p. S16). As an order of magnitude estimate, this is sufficiently large to satisfy $k \geq 10^2$ M^{-1} s^{-1} and provide justification for the assumption that the electron transfer reaction is fast on the diffusional timescales.

Comparing transient techniques employing the Cottrell equation to the steady-state method outlined above, we found that transient chronoamperometry gave a value for the apparent electron diffusion coefficient five times larger than the steady-state method ($D_e^{app}/D_e = 5$). Markedly, transient experiments are affected to a greater extent by unaccounted electromigration of both counter ions and electron hopping. Such a result is expected, since under transient conditions, there is an additional source that could contribute to an electrostatic potential gradient in the film. As shown above, a low concentration of ionic species compared to the redox-active linkers will contribute to this effect,

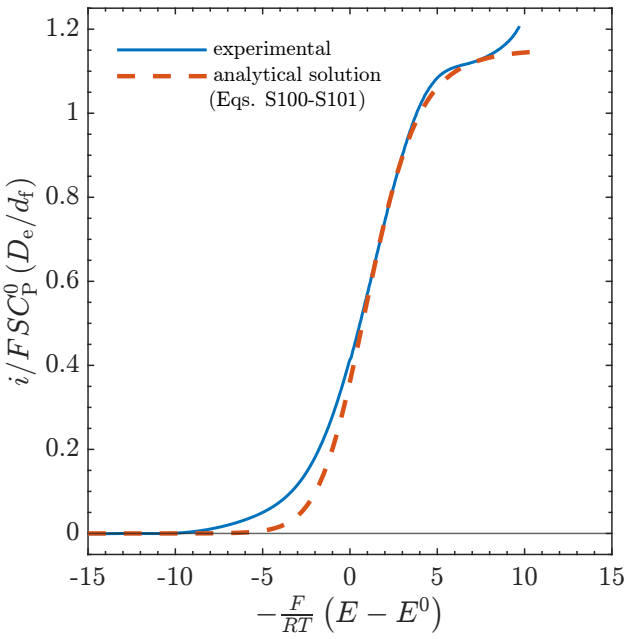

Figure 5: Dimensionless catalytic CV (solid blue line, baseline corrected) in the presence of 36 mM $[Co(bpy)_3]^{3+}$ at 50 mV s^{-1} in DMF with 0.5 M $LiClO_4$, fitted with the analytical solution to the current response (red dotted line) given by Eqs. S100-S101, Supporting Information. The plateau current yielded a steady-state value for the electron-hopping diffusion coefficient: $D_e = 5.5 \times 10^{-10}$ cm^2 s^{-1}. Other parameters used as input: $k_s^0 = 1 \times 10^{-5}$ cm s^{-1}, $\alpha = 0.5$, $n = +3$, $z = 0$, $C_P^0 = 1$ M, $C_I^0 = 0.5$ M, $d_f = 1$ μm, $E^0 = -0.5$ V, where n and z are the charges on the oxidized form of $[Co(bpy)_3]^{3+}$ and the NDI linkers, respectively. Dimensionless current and potential are defined as $\psi = i/FSC_P^0(D_e/d_f)$ and $\xi = -F/RT(E - E^0)$ respectively.

but slow ion diffusion is also a possible cause, only present in transient measurements.

This aligns with the theoretical results present in Figure 4 (see also Figure S11), as well as with previous observations made by Savéant[52] and Faulkner[25] for transient experiments conducted on closely related redox polymers. A non-zero potential gradient in the film (whether arising from slow ion movement or a weakly supported system) induces an electric field that acts to enhance the rate of electron hopping, concurrently producing a larger current response. As a result, macroscopic ion transport tends to influence measurements of D_e in the opposite way as commonly thought: its measured value is larger compared to the case of purely diffusion, rather than reflecting the slower process (electron vs. ion diffusion) in the sense of a rate-limiting step. However, D_e may still be a function of the nature of the mobile counter ion through microscopic mechanisms such as solvation,[53] ion pairing, and ion-coupled electron transfer.[16,47,54–57] Mi-

croscopic effects are discussed in more detail in the Supporting Information (Section 2).

We have addressed challenges related to transient measurements, particularly counterion diffusion and electric field effects (electromigration). These effects are neither considered in the assumptions underlying the derivation of the Cottrell equation nor experimentally controlled in transient techniques. In such cases, the measured quantity will include errors linked to unaccounted variables or physical processes.

The methodology presented here applies two strategies: exert more control over the experimental conditions and broaden the theoretical model employed to interpret the data. Introducing a mobile electron acceptor to the system and controlling operational parameters, such as scan rate and concentrations, establishes an electrochemical steady state, which yields a measurement of D_e that mitigates the effect of the counter ion's diffusivity. Addition of molecular donors/acceptors into the bulk electrolyte is relatively easy to implement and replicates a source-drain electrode configuration under the conditions outlined above. Furthermore, our extended physical model considers the influence of electromigration on the transport of mobile counter ions and electron hopping. Thus, we isolate contributions from both counter ion diffusion and electromigration from our measurements of electron hopping diffusion coefficients for planar MOF films.

Conclusion

Through the introduction of a freely diffusing electron-acceptor, we developed a steady-state measurement of electron-hopping diffusion coefficients for planar MOF films by analyzing the current response from cyclic voltammetry. Considering that redox-active MOFs often can be obtained as planar films,[58] typically with a thickness of a few microns, we expect this methodology will be amenable to a wide range of MOFs (and circumvents the need for MOF deposition on an IDA electrode).

Two independent measurements of the electron-hopping diffusion coefficient shows that *steady-state* measurements generally give values that more accurately reflect the rate of electron diffusion. Because the measurement is conducted at steady state, this evaluation minimizes any contribution from the diffusivity of the mobile counter ions, since there is no net ionic flux across the film. Interestingly, the corresponding transient measurement resulted in an apparent value for D_e that was five times larger than the one obtained by the steady-state method.

Using a physico-mathematical model, we were also able to correct for the contribution of electromigration to electron hopping, which causes an overestimation of measured diffusion coefficients compared to in the absence of field effects. When dealing with only macroscopic transport, this corrects the erroneous view that the rate of electron hopping reflects a "rate-limiting step," often considered to be either electron or ionic diffusion. In fact, we have shown that a non-zero electric field within the MOF film increases the flux of electron hopping due to electromigration, and gives rise to a larger current response. This highlights the need to develop new theoretical models, specifically tailored to the characteristics of individual experimental systems, to accurately characterize the conduction properties of redox-active MOFs. Similar approaches have been successfully applied in the study of ion insertion into conducting porous materials[59] as well as gas diffusion or porous electrocatalysts.[60]

Electron-hopping diffusion coefficients obtained at steady-state are also more relevant to the conditions found in catalytic applications, where the steady-state current is of most interest. This is particularly important for eventual applications of molecular catalysts imbedded in metal-organic frameworks that mediate the electrochemical conversion of small molecules.

Supplemental Information

Experimental methods, summary of Poisson-Nernst-Planck theory applied to electron-hopping, physico-mathematical model and derivations, summary of parameters and symbols, film characterization, and further electrochemical experiments.

Author Information

Corresponding Authors

Ben A. Johnson – *Technical University of Munich (TUM), Campus Straubing for Biotechnology and Sustainability, Uferstraße 53, Straubing 94315, Germany*; orcid.org/0000-0002-6570-6392; Email: ben.johnson@tum.de

Sascha Ott – *Department of Chemistry – Ångström Laboratory, Uppsala University, Box 523, 75237 Uppsala, Sweden*; orcid.org/0000-0002-1691-729X; Email: Sascha.Ott@kemi.uu.se

Authors

Ashleigh T. Castner – *Department of Chemistry – Ångström Laboratory, Uppsala University, Box 523, 75237 Uppsala, Sweden*; orcid.org/0000-0002-8732-6470

Hemlata Agarwala – *Technical University of Munich (TUM), Campus Straubing for Biotechnology and Sustainability, Uferstraße 53, Straubing 94315, Germany*; orcid.org/0000-0001-7347-3093

Author Contributions

CRediT author statement[61] – *Conceptualization*: B.A.J. and S.O.; *Methodology*: B.A.J.; *Formal analysis*: B.A.J.; *Investigation*: B.A.J., A.T.C., and H.A.; *Writing - Original Draft*: B.A.J.; *Writing - Review & Editing*: B.A.J., H.A., and S.O.; *Visualization*: B.A.J.; *Supervision*: S.O.; *Funding acquisi-*

tion: S.O; B.A.J. formulated and solved the physico-mathematical model.

Acknowledgments

Financial support was provided bv the European Research Council via Project ERC-CoG2015-681895 _MOFcat, the Swedish Energy Agency (42029-2), and the Swedish Research Council (2023-03395). H.A. gratefully acknowledges the Leibniz Supercomputing Centre for funding the project "pn52ha" by providing computing time and support on its Linux-Cluster.

Declaration of Interest

The authors declare no competing interests.

Declaration of generative AI and AI-assisted technologies

During the preparation of this work, the authors used ChatGPT3 in order to edit and revise grammar and sentence structure. After using this tool, the authors reviewed and edited the content as needed and take full responsibility for the content of the publication.

References

(1) Ren, S.; Joulié, D.; Salvatore, D.; Torbensen, K.; Wang, M.; Robert, M.; Berlinguette, C. P. Molecular electrocatalysts can mediate fast, selective CO_2 reduction in a flow cell. *Science* **2019**, *365*, 367–369.

(2) Wang, M.; Torbensen, K.; Salvatore, D.; Ren, S.; Joulié, D.; Dumoulin, F.; Mendoza, D.; Lassalle-Kaiser, B.; Işci, U.; Berlinguette, C. P.; Robert, M. CO_2 electrochemical catalytic reduction with a highly active cobalt phthalocyanine. *Nat. Commun.* **2019**, *10*, 3602.

(3) Zhanaidarova, A.; Jones, S. C.; Despagnet-Ayoub, E.; Pimentel, B. R.; Kubiak, C. P. Re(tBu-bpy)$(CO)_3$Cl Supported on Multi-Walled Carbon Nanotubes Selectively Reduces CO_2 in Water. *J. Am. Chem. Soc.* **2019**, *141*, 17270–17277.

(4) Costentin, C.; Savéant, J.-M. Molecular approach to catalysis of electrochemical reaction in porous films. *Curr. Opin. Electrochem.* **2019**, *15*, 58–65.

(5) Zhou, H.-C.; Long, J. R.; Yaghi, O. M. Introduction to Metal–Organic Frameworks. *Chem. Rev.* **2012**, *112*, 673–674.

(6) Lin, S.; Usov, P. M.; Morris, A. J. The role of redox hopping in metal–organic framework electrocatalysis. *Chem. Commun.* **2018**, *54*, 6965–6974.

(7) Grissom, T. G.; Sharp, C. H.; Usov, P. M.; Troya, D.; Morris, A. J.; Morris, J. R. Benzene, Toluene, and Xylene Transport through UiO-66: Diffusion Rates, Energetics, and the Role of Hydrogen Bonding. *J. Phys. Chem. C* **2018**, *122*, 16060–16069.

(8) Hod, I.; Deria, P.; Bury, W.; Mondloch, J. E.; Kung, C.-W.; So, M.; Sampson, M. D.; Peters, A. W.; Kubiak, C. P.; Farha, O. K.; Hupp, J. T. A porous proton-relaying metal-organic framework material that accelerates electrochemical hydrogen evolution. *Nat. Commun.* **2015**, *6*, 8304.

(9) Sharp, C. H.; Bukowski, B. C.; Li, H.; Johnson, E. M.; Ilic, S.; Morris, A. J.; Gersappe, D.; Snurr, R. Q.; Morris, J. R. Nanoconfinement and mass transport in metal–organic frameworks. *Chem. Soc. Rev.* **2021**, *50*, 11530–11558.

(10) Andrieux, C.; Savéant, J. Electron transfer through redox polymer films. *J. Electroanal. Chem. Interf. Electrochem.* **1980**, *111*, 377–381.

(11) Laviron, E. A multilayer model for the study of space distributed redox modified electrodes: Part I. Description and discussion of the model. *J. Electroanal. Chem. Interf. Electrochem.* **1980**, *112*, 1–9.

(12) Johnson, B. A.; Beiler, A. M.; McCarthy, B. D.; Ott, S. Transport Phenomena: Challenges and Opportunities for Molecular Catalysis in Metal–Organic Frameworks. *J. Am. Chem. Soc.* **2020**, *142*, 11941–11956.

(13) Celis-Salazar, P. J.; Cai, M.; Cucinell, C. A.; Ahrenholtz, S. R.; Epley, C. C.; Usov, P. M.; Morris, A. J. Independent Quantification of Electron and Ion Diffusion in Metallocene-Doped Metal–Organic Frameworks Thin Films. *J. Am. Chem. Soc.* **2019**, *141*, 11947–11953.

(14) Cai, M.; Loague, Q.; Morris, A. J. Design Rules for Efficient Charge Transfer in Metal–Organic Framework Films: The Pore Size Effect. *J. Phys. Chem. Lett.* **2020**, 702–709.

(15) Goswami, S.; Hod, I.; Duan, J. D.; Kung, C.-W.; Rimoldi, M.; Malliakas, C. D.; Palmer, R. H.; Farha, O. K.; Hupp, J. T. Anisotropic Redox Conductivity within a Metal–Organic Framework Material. *J. Am. Chem. Soc.* **2019**, *141*, 17696–17702.

(16) Castner, A. T.; Su, H.; Svensson Grape, E.; Inge, A. K.; Johnson, B. A.; Ahlquist, M. S. G.; Ott, S. Microscopic Insights into Cation-Coupled Electron Hopping Transport in a Metal–Organic Framework. *J. Am. Chem. Soc.* **2022**, *144*, 5910–5920.

(17) Cottrell, F. G. Der Reststrom bei galvanischer Polarisation, betrachtet als ein Diffusionsproblem. *Zeitschrift für Physikalische Chemie* **1903**, *42U*, 385–431.

(18) Chidsey, C. E. D.; Murray, R. W. Electroactive Polymers and Macromolecular Electronics. *Science* **1986**, *231*, 25–31.

(19) Pickup, P. G.; Murray, R. W. Redox conduction in mixed-valent polymers. *J. Am. Chem. Soc.* **1983**, *105*, 4510–4514.

(20) Chidsey, C. E.; Feldman, B. J.; Lundgren, C.; Murray, R. W. Micrometer-spaced platinum interdigitated array electrode: fabrication, theory, and initial use. *Anal. Chem.* **1986**, *58*, 601–607.

(21) Brodsky, C. N.; Bediako, D. K.; Shi, C.; Keane, T. P.; Costentin, C.; Billinge, S. J. L.; Nocera, D. G. Proton–Electron Conductivity in Thin Films of a Cobalt–Oxygen Evolving Catalyst. *ACS Appl. Energy Mater.* **2019**, *2*, 3–12.

(22) Gschwind, W.; McCarthy, B. D.; Suremann, N. F.; Ott, S. The Influence of Water in the Vapor-Assisted Conversion Synthesis of UiO-67 MOF Thin Films. *Eur. J. Inorg. Chem.* **2023**, *26*, e202300216.

(23) Borysiewicz, M. A.; Dou, J.-H.; Stassen, I.; Dincă, M. Why conductivity is not always king – physical properties governing the capacitance of 2D metal–organic framework-based EDLC supercapacitor electrodes: a $Ni_3(HITP)_2$ case study. *Faraday Discuss.* **2021**, *231*, 298–304.

(24) Boström, H. L. B.; Emmerling, S.; Heck, F.; Koschnick, C.; Jones, A. J.; Cliffe, M. J.; Al Natour, R.; Bonneau, M.; Guillerm, V.; Shekhah Osama and Eddaoudi, M.; Lopez-Cabrelles, J.; Furukawa, S.; Romero-Angel, M.; Martí-Gastaldo, C.; Yan, M.; Morris, A. J.; Romero-Muñiz, I.; Xiong, Y.; Platero- Prats, A. E.; Roth, J.; Queen, W. L.; Mertin, K. S.; Schier, D. E.; Champness, N. R.; Yeung, H. H.-M.; Lotsch, B. V. How reproducible is the synthesis of Zr–porphyrin metal–organic frameworks? An interlaboratory study. *Adv. Mater.* **2023**, 2304832.

(25) Chen, X.; He, P.; Faulkner, L. R. Electron transport dynamics in thin polymer films containing tris(2,2′-bipyridine)osmium(III/II) complexes. *J. Electroanal. Chem. Interf. Electrochem.* **1987**, *222*, 223–242.

(26) Wade, C. R.; Li, M.; Dincă, M. Facile Deposition of Multicolored Electrochromic Metal-Organic Framework Thin Films. *Angew. Chem. Int. Ed.* **2013**, *52*, 13377–13381.

(27) Wade, C. R.; Corrales-Sanchez, T.; Narayan, T. C.; Dincă, M. Postsynthetic tuning of hydrophilicity in pyrazolate MOFs to modulate water adsorption properties. *Energy Environ. Sci.* **2013**, *6*, 2172–2177.

(28) Kumar, A.; Li, J.; Inge, A. K.; Ott, S. Electrochromism in Isoreticular Metal–Organic Framework Thin Films with Record High Coloration Efficiency. *ACS Nano* **2023**, *17*, 21595–21603.

(29) Li, J.; Kumar, A.; Johnson, B. A.; Ott, S. Experimental manifestation of redox-conductivity in metal-organic frameworks and its implication for semiconductor/insulator switching. *Nat. Commun.* **2023**, *14*, 4388.

(30) Liu, W.; Xu, W.; Lin, J. L.; Xie, H. Z. Tris(2,2′-bipyridine-κ^2 N:N′)cobalt(III) trichloride tetrahydrate. *Acta Cryst. E* **2008**, *64*, m1586.

(31) Johnson, B. A.; Ott, S. Diagnosing surface versus bulk reactivity for molecular catalysis within metal–organic frameworks using a quantitative kinetic model. *Chem. Sci.* **2020**, *11*, 7468–7478.

(32) Damköhler, G. Einflüsse der Strömung, Diffusion und des Wärmeüberganges auf die Leistung von Reaktionsöfen.: I. Allgemeine Gesichtspunkte für die Übertragung eines chemischen Prozesses aus dem Kleinen ins Große. *Zeitschrift für Elektrochemie und angewandte physikalische Chemie* **1936**, *42*, 846–862.

(33) Thiele, E. W. Relation between Catalytic Activity and Size of Particle. *Ind. Eng. Chem.* **1939**, *31*, 916–920.

(34) Andrieux, C. P.; Dumas-Bouchiat, J. M.; Savéant, J. M. Catalysis of electrochemical reactions at redox polymer electrodes. Kinetic model for stationary voltammetric techniques. *J. Electroanal. Chem.* **1982**, *131*, 1–35.

(35) Costentin, C.; Savéant, J.-M. Cyclic Voltammetry of Electrocatalytic Films: Fast Catalysis Regimes. *ChemElectroChem* **2015**, *2*, 1774–1784.

(36) Fogler, H. S., *Elements of Chemical Reaction Engineering*, 5th; Pearson Education Inc.: 2016; Chapter 15, pp 719–767.

(37) Costentin, C.; Savéant, J.-M., *Elements of Molecular and Biomolecular Electrochemistry*, 2nd ed., Hoboken, NJ, 2019.

(38) Costentin, C. Molecular Catalysis of Electrochemical Reactions. Overpotential and Turnover Frequency: Unidirectional and Bidirectional Systems. *ACS Catal.* **2021**, *11*, 5678–5687.

(39) Bard, A. J.; Faulkner, L. R., *Electrochemical Methods: Fundamental and Applications*, 2nd; John Wiley & Sons, Inc.: Hoboken, 2001.

(40) Costentin, C.; Savéant, J.-M. Cyclic Voltammetry Analysis of Electrocatalytic Films. *J. Phys. Chem. C* **2015**, *119*, 12174–12182.

(41) Aoki, K.; Tokuda, K.; Matsuda, H. Theory of linear sweep voltammetry with finite diffusion space. *J. Electroanal. Chem. Interf. Electrochem.* **1983**, *146*, 417–424.

(42) We define $E_{1/2}$ as the potential value at half the plateau current, valid for a sigmoidal voltametric response; this is not strictly a thermodynamic property, especially with multi-electron catalytic reactions.

(43) Menshykau, D.; Compton, R. G. Electrodes Modified with Electroinactive Layers: Distinguishing Through-Film Transport from Pinhole (Pore) Diffusion. *Langmuir* **2009**, *25*, 2519–2529.

(44) Costentin, C.; Savéant, J.-M. Cyclic voltammetry of fast conducting electrocatalytic films. *Phys. Chem. Chem. Phys.* **2015**, *17*, 19350–19359.

(45) Newman, J.; Thomas-Alyea, K. E., *Electrochemical Systems*; Wiley: 2004.

(46) Savéant, J. M. Electron hopping between fixed sites: Equivalent diffusion and migration laws. *J. Electroanal. Chem. Interf. Electrochem.* **1986**, *201*, 211–213.

(47) Savéant, J. M. Electron hopping between localized sites: effect of ion pairing on diffusion and migration; general rate laws and steady-state responses. *J. Phys. Chem.* **1988**, *92*, 4526–4532.

(48) Schröder, U.; Oldham, K. B.; Myland, J. C.; Mahon, P. J.; Scholz, F. Modelling of solid state voltammetry of immobilized microcrystals assuming an initiation of the electrochemical reaction at a three-phase junction. *J. Solid State Electrochem.* **2000**, *4*, 314–324.

(49) Yan, M.; Johnson, E. M.; Morris, A. J. Redox Hopping in Metal–Organic Frameworks through the Lens of the Scholz Model. *J. Phys. Chem. Lett.* **2023**, *14*, 10700–10709.

(50) Monnier, V.; Odobel, F.; Diring, S. Exploring the Impact of Successive Redox Events in Thin Films of Metal–Organic Frameworks: An Absorptiometric Approach. *J. Am. Chem. Soc.* **2023**, *145*, 19232–19242.

(51) Chidsey, C. E. D.; Murray, R. W. Redox capacity and direct current electron conductivity in electroactive materials. *J. Phys. Chem.* **1986**, *90*, 1479–1484.

(52) Andrieux, C. P.; Savéant, J. M. Electroneutrality coupling of electron hopping between localized sites with electroinactive counterion displacement. 1. Potential-step plateau currents. *J. Phys. Chem.* **1988**, *92*, 6761–6767.

(53) Huang, J.; Marshall, C. R.; Ojha, K.; Shen, M.; Golledge, S.; Kadota, K.; McKenzie, J.; Fabrizio, K.; Mitchell, J. B.; Khaliq, F.; Davenport, A. M.; LeRoy, M. A.; Mapile, A. N.; Debela, T. T.; Twight, L. P.; Hendon, C. H.; Brozek, C. K. Giant Redox Entropy in the Intercalation vs Surface Chemistry of Nanocrystal Frameworks with Confined Pores. *J. Am. Chem. Soc.* **2023**, *145*, 6257–6269.

(54) Savéant, J.-M. Evidence for Concerted Pathways in Ion-Pairing Coupled Electron Transfers. *J. Am. Chem. Soc.* **2008**, *130*, 4732–4741.

(55) Anson, F. C.; Blauch, D. N.; Savéant, J. M.; Shu, C. F. Ion association and electric field effects on electron hopping in redox polymers. Application to the tris(2,2'-bipyridine)osmium(3+)/tris(2,2'-bipyridine)osmium(2+) couple in Nafion. *J. Am. Chem. Soc.* **1991**, *113*, 1922–1932.

(56) Savéant, J. M. Electron hopping between localized sites: coupling with electroinactive counterion transport. *J. Phys. Chem.* **1988**, *92*, 1011–1013.

(57) Bazant, M. Z. Unified quantum theory of electrochemical kinetics by coupled ion–electron transfer. *Faraday Discuss.* **2023**, *246*, 60–124.

(58) Hod, I.; Bury, W.; Karlin, D. M.; Deria, P.; Kung, C.-W.; Katz, M. J.; So, M.; Klahr, B.; Jin, D.; Chung, Y.-W.; Odom, T. W.; Farha, O. K.; Hupp, J. T. Directed Growth of Electroactive Metal-Organic Framework Thin Films Using Electrophoretic Deposition. *Adv. Mater.* **2014**, *26*, 6295–6300.

(59) Costentin, C. Cyclic Voltammetry to Study Dynamics of Ion Insertion in Porous Materials. *Adv. Energy Sustainability Res.* **2024**, *5*, 2300242.

(60) Moore, T.; Xia, X.; Baker, S. E.; Duoss, E. B.; Beck, V. A. Elucidating Mass Transport Regimes in Gas Diffusion Electrodes for CO_2 Electroreduction. *ACS Energy Lett.* **2021**, *6*, 3600–3606.

(61) Brand, A.; Allen, L.; Altman, M.; Hlava, M.; Scott, J. Beyond authorship: attribution, contribution, collaboration, and credit. *Learned Publishing* **2015**, *28*, 151–155.